Properties of Diamond Nanomaterials

17

Tad Whiteside, Clifford Padgett, and Amanda Mcguire

Keywords

Carbon nanoflims • Carbon nanostructures • Carbon nanotubes • Diamond nanoflims • Diamond nanoparticles • Diamond nanorods • Diamond nanostructures • Diamond nanowires

Introduction

Nanosized diamond represents an important division of carbon nanostructures and has a large number of potential uses in many areas of science and technology, such as molecular-scale computing devices, drug delivery, material coatings, and reinforcing agents in composite material. Diamond nanostructures are defined as sp^3-hybridized carbon atoms bound to other sp^3-hybridized carbon atoms whose size in the largest performance-sensitive dimension is typically less than 100 nm. Within this division of materials there exist three primary classes or '*dimensionalities*': pseudo-zero dimensional diamond nanoparticles, one-dimensional diamond nanowires, and two-dimensional diamond nanofilms. In this article, we present an overview of the sizes of the materials, their current and proposed uses, the methods of synthesis and characterization, and their various properties.

T. Whiteside (✉)
Savannah River National Laboratory, Aiken, SC, USA
e-mail: tad.whiteside@srnl.doe.gov

C. Padgett • A. Mcguire
Department of Chemistry and Physics, Armstrong Atlantic State University, Savannah, GA, USA
e-mail: clifford.padgett@armstrong.edu; am5232@students.armstrong.edu

B. Bhushan et al. (eds.), *Handbook of Nanomaterials Properties*,
DOI 10.1007/978-3-642-31107-9_43,

Diamond Nanoparticles

Diamond nanoparticles typically range from 2 to 100 nm in size. They are created by multiple means and have many unique uses. Most diamond nanoparticles have a diamond (sp^3) carbon core and are surrounded by an amorphous (sp^2) carbon shell. These nanoparticles have found uses as reinforcing agents in composite material, as drug delivery systems, as biological imaging agents, and as catalysts.

Synthesis

Diamond nanoparticles have been synthesized using several techniques, such as explosive detonation, chemical vapor deposition, plasma vapor deposition, laser ablation, hydrodynamic cavitation, and irradiation of other forms of carbon with ions or electrons. Bulk synthesis of diamond nanoparticles is produced by detonation of explosives (containing excess carbon relative to the amount of oxygen present). In this process, diamond nanoparticles are synthesized in the high-pressure-high-temperature conditions found within the shock wave created during detonation. Under these conditions, diamond nanoparticles between 3 and 5 nm are typically found in the soot, which can be up to 80 % by weight in diamond nanoparticles [1–4].

Diamond nanoparticles have also been synthesized from carbon nanotubes and graphite under high-pressure-high-temperature methods [5]. Using these methods, diamond nanoparticles exhibit higher oxygen content than ones made from graphite (7.34 % vs. 5.8 %). It is believed that this is due to the carbon nanotube structure, which is more likely to contain oxygen than the structure of graphite [6]. As a result, the properties of these diamond nanoparticles may have enhanced biological applications [7].

Cavitation experiments have shown that diamond nanoparticles can be successfully created in a reproducible manner using a carbon-containing contact liquid. Hydrodynamic cavitation provides a new way to control impurities, defects, structure, size, and other properties. The physics of cavitation bubbles collapsing and of shock wave compression (detonation) is very similar and allows for investigation of the rapid cooling process in detonation experiments, which is known to be important in the formation of diamond nanoparticles [8]. The hydrodynamic cavitation of benzene generated diamond nanoparticles, which range from 5 to 20 nm, as well as aggregates of other carbon nanostructures [8].

Pulsed laser-induced liquid–solid interfacial reaction has been used to generate diamond nanoparticles in various shapes including cubic and hexagonal structures [9–14]. The mechanism of this laser-based material processing method for the nucleation and growth of the diamond nanoparticles is not well understood. The diamond nanoparticles form via the condensation of water on the ablated graphite, which is formed by a laser-induced plasma at the liquid–solid interface. This system reaches pressures in the range of 10–15 GPa and temperatures in the range of 4,000–5,000 K [10].

Characterization

Diamond nanoparticles are generally characterized in one of two states: either dispersed into a solution or incorporated into a composite material. The most common characterizing methods are microscopy (atomic force microscopy (AFM), scanning electron microscopy (SEM), and/or transmission electron microscopy (TEM)); spectroscopy (UV–vis, FTIR, and X-ray photoelectron spectroscopy (XPS)); and crystallography (X-ray diffraction (XRD)). Other characterization techniques, such as thermogravimetric analysis (TGA), have also been used.

AFM/SEM/TEM

AFM is used to probe the surface topography of the diamond nanoparticles [15, 16]. These results can characterize the diamond nanoparticle grain size in composite structures as well as the thickness and roughness of the composite film [16]. SEM and TEM images provide details of the morphologies (shape/structure) of the nanoparticles as well as their dispersion on the substrate or within a composite [15–21]. These images are used to examine how these morphologies change as synthesis methods change [20]. They are also used to characterize the impurities or other structures present within the composite materials [17].

UV–Vis

UV–vis spectroscopy is used to characterize diamond nanoparticle dispersions and films [17, 22, 23]. For diamond nanoparticles, the absorption dies off rapidly (transmittance increases) at wavelengths greater than 200 nm. When these particles are annealed at high (+1,000 K) temperatures, the diamond cores turn into fullerene-like carbon onions, and an absorption peak around 263 nm appears. This is due to the increase in sp^2 sites and a corresponding decrease in sp^3 sites [17, 22].

FTIR

FTIR spectroscopy is used to track the changes in functionalization of the surface of diamond nanoparticles as experimental conditions change [19, 24]. It is also used to measure the types of bonds formed between the nanoparticles and their surroundings [25]. For example, to determine if diamond nanoparticles are chemically bonded to ethylenediamine, there should be bands present in the FTIR spectra. If they are only adsorbed onto ethylenediamine, these bands will be missing. The FTIR spectra show the bands; thus, diamond nanoparticles bond to ethylenediamine [25].

XRD

The typical XRD pattern of diamond nanoparticles shows sharp peaks at approximately 42, 75, and 95 2θ which correspond to the (111), (220), and (311) facets of diamond; see Fig. 17.1 [7, 15, 16]. If the diamond nanoparticles are embedded in an amorphous matrix, the XRD peaks will be very broad or absent [16].

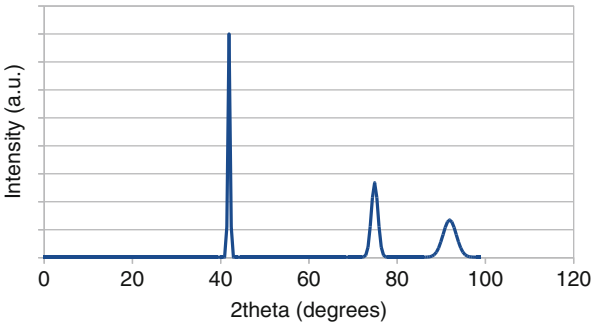

Fig. 17.1 XRD spectra of diamond nanoparticles

TGA

Thermogravimetric analysis is a complementary method to FTIR and is used to provide additional information in support of the description of the composition of functionalized diamond nanoparticles [24, 25].

Properties

Biological

Diamond nanoparticles have been conjugated with many different biomolecules, including nucleic acids, proteins, and biotins [26]. These conjugated systems retain much of their functionality and activity, and it has been shown that they can actively target specific cells and organs [26]. One example of this conjugation is the adsorption of the proteins albumin, γ-globulin, and lysozyme onto 5 nm and 100 nm diamond nanoparticles. This conjugation was measured using FTIR [27], and it was shown that these proteins most readily adsorb onto the 5 nm nanoparticles due to their larger surface area [27]. Additionally, this adsorption causes changes in the FTIR spectra, particularly those spectra of the 5 nm nanoparticles, which is most likely due to structural deformations of the adsorbed protein [27]. Diamond nanoparticles created from carbon nanotubes under high pressure and high temperature have more oxygen-containing functional groups than diamond nanoparticles prepared from graphite [7]. These nanoparticles have a negative charge of −27 mV and as such bond readily with dopamine. When these dopamine-diamond nanoparticles were placed in water, they formed a stable (2-day) suspension, compared to a diamond nanoparticle suspension which was only stable for 7 h [7]. Analysis via small-angle X-ray scattering spectroscopy suggests that the dopamine-diamond nanoparticles have an 11.4 % smaller surface interface than diamond nanoparticles [7].

Diamond nanoparticles are efficient biological imaging agents in that they are bright emitters with a high efficiency and do not exhibit photobleaching or blinking [26]. These properties allow the tracking of single particles within cells by the use of one- or two-photon excitation [26].

Diamond nanoparticles can be added to cells in concentrations up to 400 μg mL^{-1} without showing reduction in activity [26]. The cytotoxicity of nanodiamond has also been measured against mitochondrial function, luminescent ATP production, osteoblast differentiation, and others. None of these processes show a reduction in cell viability [21, 26].

Chemical

When diamond nanoparticles are incorporated into a Ni-P composite, the composite structure has excellent corrosion resistance as compared to conventional Ni-P structures [16]. This is likely due to the nanodiamond particles lowering the chemical activity of the Ni-P film [16].

Mechanical

Diamond nanoparticles have been incorporated into liquid paraffin at 0.2 % by weight. This incorporation caused a decrease in the friction coefficient by approximately 0.01 (from 0.09 to 0.08) [19]. A similar decrease is seen when diamond nanoparticles are incorporated into Ni-P films and in TiO_2 films [15, 16]. In the TiO_2 films, when nanodiamond is added at more than 1 % by weight, the coefficient of friction increases. This is likely due to the synthesis technique used to create the diamond-TiO_2 composite [15].

Functionalizing the surface of diamond nanoparticles generally increases the stiffness and hardness of the material the functionalized nanodiamond is incorporated into. When diamond nanoparticles are doped with amines or carboxylic acid and mixed with an epoxy resin, these particles react with the resin to covalently incorporate the nanodiamond particle into the polymer network [25]. For 7 % by weight nanodiamond-amines, this incorporation improved the Young's modulus of the epoxy from 0.3 to 3.0 GPa and the hardness from 0.5 to 90 MPa [25]. For 7 % by weight nanodiamond-carboxylic acid, the Young's modulus increased to 2.0 GPa and the hardness increased to 30 MPa [25]. When diamond nanoparticles were incorporated into another polymer, poly(L-lactic acid) (PLLA), the Young's modulus was also observed to increase from 2.6 to 6.8 GPa at 7 % by weight nanodiamond [21]. The hardness also increased from 0.05 to 0.31 GPa [21]. When diamond nanoparticles are incorporated into Ni-P films, the hardness of those films is also observed to increase [16].

Optical

Diamond nanoparticles synthesized such that vacancies are next to nitrogen impurities create color centers that have strong fluorescence and are resistant to photobleaching [26, 28, 29].

Diamond nanoparticles are weak optical limiters (where the transmittance of a material reaches a constant value, even as light intensity increases) [17]. The transmittance of diamond nanoparticles is also limited through an applied voltage. In polymer-dispersed liquid crystals (PDLC), diamond nanoparticles limit the transmittance as a voltage is applied across the film [30]. For undoped PDLC,

the transmittance increases from 0 % to 60 % as the voltage increases to 100 V and then levels off as the voltage increases beyond 100 V [30]. For PDLC doped with 1 % by weight diamond nanoparticles, the transmittance increases to 40 % as voltage increases to 40 V and then levels off as the voltage is increased [30].

The refractive index of a poly(vinyl alcohol) (PVA) polymer film increases with increasing quantities of embedded diamond nanoparticles [23]. The refractive index increases linearly from 1.52 for pure PVA to 1.88 for 60 % by volume diamond nanoparticles [23]. These are similar results to those found in Vlaeva et al. [31]. In the work of Vlaeva et al. [31], the PVA's refractive index increases from 1.488 to 1.505 at 1 % by weight diamond nanoparticles [31].

Physical

When 0.67 % by weight diamond nanoparticles are added to an epoxy resin, the dielectric permittivity of the resin decreases by approximately 1.5 from 5.75 to 4.25 [18]. This decrease is due to the diamond nanoparticles causing an increase in the number of cross-links to be formed during the resin's curing process, thereby strengthening the resin and disabling its ability to orient under an applied electric field [18]. Similar results are noted when diamond nanoparticles are added to a benzocyclobutene film. In this case, the permittivity decreases from 2.65 to 2.5 to 2.25 as 0.5 % and 1.5 % by weight diamond nanoparticles are added to the mixture [20]. However, as the weight percent of diamond nanoparticles increases in the benzocyclobutene mixture, the relative permittivity increases. This is likely caused by the hydrophobicity of the benzocyclobutene and the surface properties of the diamond nanoparticles by creating an 'air gap' surrounding the nanoparticles [20].

Thermal

When diamond nanoparticles are incorporated into benzocyclobutene at more than 4 % by weight, an increase of thermal conductivity by 40 % is observed (from 0.23 to 0.34 W m^{-1} K^{-1}) [20].

As diamond nanoparticles are incorporated into a copper film, the thermal expansion coefficient of these films decreases, up to a 20 % by volume content of nanoparticles, after which it increases [32]. This increase is likely due to high specimen porosity and the low strength of the bond between the copper and diamond nanoparticles [32].

Diamond Nanowires

Diamond nanowires are generally defined as 'one-dimensional' structures primarily composed of sp^3-bonded carbon atoms arranged in a cylinder with a diameter size on the order of nanometers and a length which ranges from nanometers to microns. These materials are usually created through an etching process and can be functionalized to improve their bonding and use in composite materials.

While the use of diamond nanowires in applications is still at the experimental stage, they have many potential uses, including as components of molecular-scale computing devices, as reinforcing agents to be mixed with polymers, and as thermal management materials.

Synthesis

Diamond nanowires are created through a variety of techniques, primarily through etching diamond film or through the growth from diamond nucleation sites. The original description in the literature used air plasma to etch remove a polycrystalline diamond film coated with a molybdenum mask to form well-aligned, uniformly dispersed diamond nanowires up to 60 nm in diameter [33]. Another method creates diamond nanowires on the order of 50–200 nm in diameter and several microns in length by reactive-ion etching single-crystal diamond substrates using oxide or aluminum impurities within the substrate, each of which acts as a micro-mask [34]. Diamond nanowires can also be created by using gold nanodots as the etching mask in a hydrogen/argon plasma [35].

Most plasma-assisted etching methods use a mask to protect the carbon underneath the mask [33–35]. In 2009, a 'mask-free' process to fabricate an array of boron-doped diamond nanowires was reported. The described mechanism had boron oxide form on the surface of the film and then serve as the etching mask during this process [36]. However, it was later shown that diamond nanowire arrays could be fabricated using the same mask-free process without boron [37, 38]. In fact, very long aligned one-dimensional (submicron) diamond nanowires have been reported using mask-free processes from a polished polycrystalline substrate and oxygen plasma etching [39]. It should be noted that in the 'mask-free' etching process, the mask is generally self-generating. In the case of Lin et al. [39], the mask is Fe_2O_3, generated from the steel substrate holder.

A growth technique uses microwave plasma-assisted chemical vapor deposition with the aid of an anodic aluminum oxide template and 50 nm diamond nanoparticle nucleation sites to create arrays of polycrystalline diamond nanowires 300 nm in diameter and up to 5 μm long [40]. Smaller diamond nanowires have been synthesized using a hydrogen plasma posttreatment of multiwalled carbon nanotubes. This process resulted in single-crystalline diamond nanowires with diameters of 8–10 nm and lengths up to 200 nm. These diamond nanowires had a core-sheath structure with the outer shell being composed of amorphous carbon while the inner core was diamond. The nanowires grew along the (110) direction. The researchers proposed a growth mechanism similar to the silicon oxide-assisted growth mechanism seen in Si nanowires [41, 42]. Diamond nanowires have also been created from C_{60} fullerenes using high temperature and pressure in a multi-anvil apparatus. The individual diamond nanowires that make up the aggregates were 5–20 nm in diameter and longer than 1 μm [43]. Diamond nanowires with diameter in the range of 3–5 nm and lengths up to 200 nm have been synthesized from the hydrogen plasma posttreatment of nanocrystalline diamond films. In this

process, the diamond nanowires grow from graphite clusters that are created by the etching of carbon film (both diamond and non-diamond); these clusters then recrystallized to form nanodiamond which grew into the diamond nanowires [44]. Argon-rich microwave plasma chemical vapor deposition containing nitrogen and methane has been used to grow diamond nanowires on Si wafers [45]. This generally produces diamond nanowires covered by amorphous carbon, but improvements in the method have resulted in increased efficiency and the generation of graphite-coated single-crystalline diamond nanowires whose core was 2–5 nm in diameter and tens of nanometers long. The graphite encapsulation was variable in thickness and was enhanced by the content of nitrogen gas used [46].

Simulated Properties

Mechanical

Simulations of diamond nanowires with different diameters and with different crystal plane orientations ((111), (011), (001)) along the axis have been carried out to predict the elastic stiffness and tensile fracture force of these materials. The results from these simulations suggest that for diamond nanowires with a diameter greater than 6 nm, the elastic stiffness and tensile fracture force would exceed that of carbon nanotubes, depending on the axial orientation of the diamond nanowire [47].

Physical

With the aid of molecular modeling and a many-body bond order potential, the binding energy for several diamond nanowires with different axial orientations was calculated, and it was shown to be comparable to that of single-walled carbon nanotubes [47].

First principle calculations have been used to determine the thermodynamic stability of diamond nanowires and their preferred morphologies. The results from these calculations suggest that the (111) facets lead to partial graphitization and that bare (001) surfaces undergo dimer pairing surface reconstructions to reduce the number of radical sites. The (011) facets largely preserve the diamond structure and result in stable diamond nanowires [48]; in addition this morphology also had the smallest calculated heat of formation [49]. Other morphologies have been explored using a bond order potential by Brenner [50] to calculate the heat of formation for structures that represent the six different morphologies corresponding to the (001) and (011) principal axes and low-index facets [51]. These calculations showed that stability is based on a combination of surface and axis orientation, which is consistent with experimental observations of diamond nanowire growth in the (011) direction [41]. Simulations of the phase stability of diamond nanowires using a heat of formation model also predict that the stability is dependent on morphology and nanowire diameter. This indicates that diamond nanowires occupy a ‘window of stability’ that ranges from 3 to 9 nm in diameter [52].

Thermal

Molecular dynamics simulations were used to calculate the thermal conductivity of diamond nanowires and the results compared to those of carbon nanotubes, using the Brenner potential [50]. In these simulations, the dependency of the thermal conductivity on length, temperature, and boundary condition was examined and the thermal conductivity was found to be extremely dependent on the nanowire (or nanotube) length, especially at the shorter lengths. The thermal conductivity of a (10, 10) nanotube varied from 215 W m^{-1} K^{-1}, for a 50 nm periodic box length, to 831 W m^{-1} K^{-1}, for a 1 μm box. Simulations of the nanowires suggest they have a much lower thermal conductivity than carbon nanotubes. This is probably due to the increased number of scattering sites on the nanowire surfaces [53]. Calculations have also shown that thermal conductivity of diamond nanowires is less affected by surface functionalization than similarly sized carbon nanotubes and that above 3 % surface functionalization diamond nanowires are better thermal conductors than carbon nanotubes. This makes them valuable for building thermal management polymers [54].

Electronic

Density functional tight-binding calculations have been used to examine the electronic properties of diamond nanowires. The result of these calculations indicates that both of these materials may exhibit metallic and semiconducting electrical properties, depending on their morphology and size. The band gap energy for all large diamond nanowires (area greater than 150 $Å^2$) was metallike with the gap energy equal to zero. Smaller nanowires had a band gap energy ranging from 0 to 0.60 eV, depending on size and morphology [48].

Measured Properties

Mechanical

The strength and hardness of aggregated diamond nanowires have been extrapolated from X-ray diffraction (XRD) data and measured using a Vickers-type indenter. The XRD data suggest that the density of aggregated diamond nanowires is 0.2–0.4 % higher than that of bulk diamond and their isothermal bulk modulus is 491 GPa (bulk diamond is 442 GPa). The indentation measurements indicate that the hardness of aggregated diamond nanowires exceeds 100 GPa. In addition, these diamond nanowires scratched the (111) faces of natural single-crystal diamond [43]. These measurements show that diamond nanowires have the lowest measured compressibility and are the densest of all carbon materials [43]. Aggregated diamond nanowires overcome many of the problems associated with the use of single-crystal diamond abrasives, such as the tendency to undergo graphitization at elevated temperature, low fracture toughness, and being directionally dependent for many of its physical properties. Aggregated diamond nanowires have a fracture toughness of 11 MPa*$m^{0.5}$, which exceeds that of both natural and synthetic diamonds (3–5 MPa*$m^{0.5}$) [55].

Aggregated diamond nanowire samples show the enhancement of wear resistance up to 300 % in comparison with commercially available polycrystalline diamonds; in addition, these diamond nanowires show no reaction with iron (to form iron carbide) that typically limits the use of diamond in the cutting of steel and other iron-containing alloys. This makes them extremely attractive materials for applications as super-abrasives [56].

Using indentation experiments and atomistic simulations, characteristic load–displacement curves have been generated and used to determine the mechanical properties of diamond nanowires. The results indicate these substances undergo elastic deformation during indentation, with the force exerted on the indenter varying as the depth raised to the power 1.6 [57]. The values from these experiments show that diamond nanowires have a similar value for hardness as diamond and the elastic modulus value exceeded that of diamond in some cases. The indentation measurements are very precise for diamond and diamond films; however, the measurements on aggregated diamond nanowires show large variation in the measured values due to inhomogeneity in the material [57].

Optical

The optical properties of diamond nanowires have been measured and compared to those of diamond and diamond films via Raman and infrared spectroscopy. In general, a strong peak around 1,332 cm^{-1} (characteristic peak of diamond) and a broad peak around 1,500–1,600 cm^{-1} are observed in the Raman spectrum of nanocrystalline diamond (corresponding to the (100) facet). The broadness of the peak is used to determine the size and purity of these nanowires and crystalline diamond [58].

Diamond Nanofilms

Diamond-like carbon (DLC) thin films are sheets of amorphous sp^2-bonded (graphite-like) carbon bound to crystalline phases of sp^3-bonded (diamond-like) carbon [59]. The size of the crystalline phases typically ranges from 5 to 50 nm, and the film's thickness is usually less than 100 nm. These films were first synthesized and characterized by Aisenberg and Chabot in the early 1970s and are typically created through chemical vapor deposition. The ratio of the sp^3 to sp^2 bonds in the carbon network determines the characteristics of the DLC films [59]. The sp^3-bonded carbons govern the mechanical properties and the sp^2-bonded carbons, which are near the Fermi level, control the electronic and optical properties [60]. Overall, these films have characteristics similar to that of macroscale diamond: optically transparent, large index of refraction, biocompatible, electrically insulating, high hardness, low friction, resistance to acid, and low dielectric constant [61].

The optical and electrical properties of DLC films make them ideal for magnetic storage media and optical coating applications. In addition, their mechanical properties of high hardness and low friction have led to much interest in using these films for coatings used in precision manufacturing and machining. After overcoming

substrate adhesion issues, many objects are now being coated with DLC films and used in areas ranging from metal cutting taps and extrusion dies to engine cam shafts and medical bone saws [62, 63]. Coating implantable medical devices with DLC films is routinely done due to their wear resistance and high biocompatibility. They have recently been fabricated as self-supporting foils at widths of less than 5 nm and used for laser-driven ion acceleration [64].

Synthesis

Many techniques have been used to create DLC films including ion beam deposition/sputter deposition (physical vapor deposition – PVD) [60, 61, 65–67], plasma-enhanced deposition from a hydrocarbon gas (chemical vapor deposition – CVD) [59, 68–77], cathodic arc [64, 78], laser ablation [79–81], and electrodeposition [82–85]. Based on a literature review, the simplest and most commonly used techniques in a research environment are CVD and electrodeposition. For commercial applications, a hybrid technique – known as closed-field unbalanced magnetron sputter ion plating – combines the PVD and CVD methods to create durable, high-quality DLC films.

The general method to create DLC films using CVD is to use glass, SnO_2-coated glass, or a monocrystalline Si wafer as the substrate. This substrate is kept at a low temperature (300–500 K) in a low-pressure (1–1,000 Pa) chamber. It is exposed to a precursor carbon source, such as methane or acetylene, and a carrier gas, like argon or nitrogen, in the presence of an energy source, such as a hot filament, microwave power, or a plasma arc discharge for less than 1 h. The ratio of carbon source to carrier gas is the primary mechanism that controls the film's creation and properties. However, these properties are also affected by the temperature, pressure, energy source, and deposition time. The CVD method is typically used to create films that range from 10 to 100 nm thick. The following references have complete details on individual experiments where the above parameters are varied and described in detail: [59, 60, 68–77, 86, 87].

When electrodeposition is used to create DLC films, the substrate is mounted at the anode and a graphite plate is mounted at the cathode within an electrolytic cell. The distance between the two plates is less than 10 mm. The electrolytic bath typically consists of an aqueous or liquid carbon source, such as methanol, DMSO, or acetic acid. The voltage used depends on the electrolytic solution and varies between 2.5 V and 800 V. The temperature of the solution is mild, ranging between 300 and 400 K. The deposition rate varies between 10 and 100 nm h^{-1}. The following references have complete experimental details: [82–85].

Characterization

DLC films are characterized using the standard techniques of microscopy and spectroscopy. The most common characterizing methods used are atomic force

microscopy (AFM), Raman spectroscopy, X-ray diffraction (XRD), and X-ray photoelectron spectroscopy (XPS). Other techniques, such as transmission electron microscopy (TEM) and scanning electron microscopy (SEM), are also used, but mainly to complement the results obtained by the previous methods.

AFM

AFM is used to determine the surface topographical information about the DLC films. AFM results also show that the substrate surface greatly influences the final DLC film topography [59]. For etched surface substrates, the final DLC film roughness decreases as deposition time increases. For substrates with a powder coating, the final DLC film roughness increased as deposition time increased. For both types of substrates, the final average surface roughness was between 20 and 50 nm [59]. This value is in keeping with the measured surface roughness by other researchers [64, 71, 75, 84].

SEM and TEM

SEM and TEM images provide details of the morphologies of the DLC films [68, 72, 74, 76, 83, 86]. Multiple SEM and TEM images can be used to examine how these morphologies change as synthesis methods change. In addition to morphologies, SEM can be used to analyze the films thickness [74, 86]. It is also used for DLC films containing dopants, to characterize the density and dispersion of the dopants [60, 85].

Raman

The composition of the DLC films can be characterized using Raman spectroscopy. A typical Raman spectrum of a DLC film has the general shape shown in Fig. 17.2. There are two distinctive primary peaks: the G-peak and the D-peak. The G-peak and D-peak terminology is from carbon nanotube (CNT) nomenclature, with the G-peak meaning 'graphitic-carbon' (sp^2 carbon) and the D-peak meaning 'disorder' (sp^3 carbon) because in CNTs, most of the atoms are sp^2 atoms and the tube ends or defects are sp^3 carbons. The G-peak occurs between 1,550 and 1,575 cm^{-1} and the intensity is a measure of the number of sp^2 sites within the film; the width of the G-peak is indicative of the environment of the sp^2 sites. A broad G-peak means the sp^2 sites are within the carbon matrix and are bonded to atoms with many different vibrational frequencies, such as sp^3 carbons and hydrogen. The D-peak occurs between 1,325 and 1,375 cm^{-1} and the intensity is a measure of the number of sp^3 sites within the film [85]. This peak also tends to be broad because the sp^3 carbons are bound to terminal hydrogens, other sp^3 carbons, sp^2 carbons, etc. The ratio of these peaks (I_D/I_G) is a measure of the amount of sp^3 sites in the carbon matrix and is used to categorize the DLC film [60]. The exact wave number of these peaks may shift due to the bonding environment [70]. There may be a peak near 1,150 cm^{-1}, which has been related to the calculated phonon density of states of diamond [68]. However, other groups have assigned it to transpolyacetylene [71], and, due to the noise in most spectra, this peak may not actually be present.

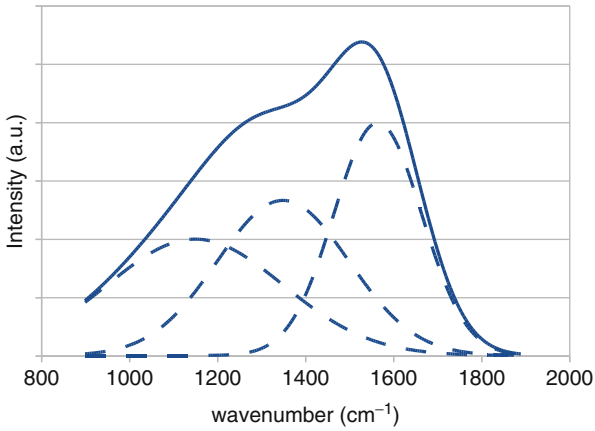

Fig. 17.2 Typical Raman spectra of DLC film obtained at 300 K

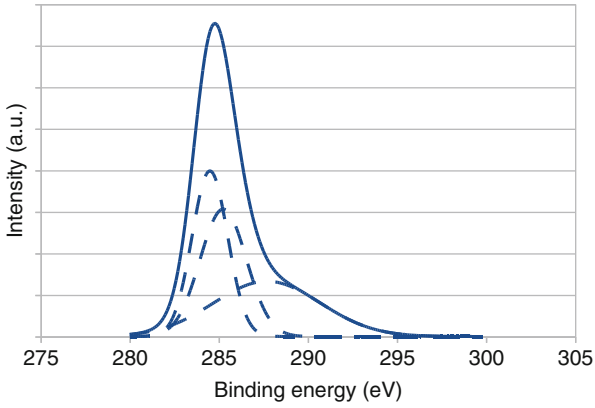

Fig. 17.3 XPS wide survey spectra of pure DLC

XPS

XPS is a useful technique to examine solid-state samples and provides an estimate of the chemical composition. A typical C_{1s} spectrum of a DLC film is shown in Fig. 17.3. The solid line is the measured values. The dashed lines are the deconvoluted peaks: the sp^2-hybridized peak is around 284.5 eV, the sp^3 hybridized is around 285 eV, and the peak around 287 is likely due to CO bonds formed by the air and the sample [67, 77, 83, 84].

XRD

The XRD patterns of the DLC films depend upon the growth conditions. A sample XRD pattern is shown in Fig. 17.4. If diamond is present, there will be peaks around 42 2θ for the (111) facet and around 75 2θ for the (220) facet. If there are no peaks, then the film is amorphous [70, 75].

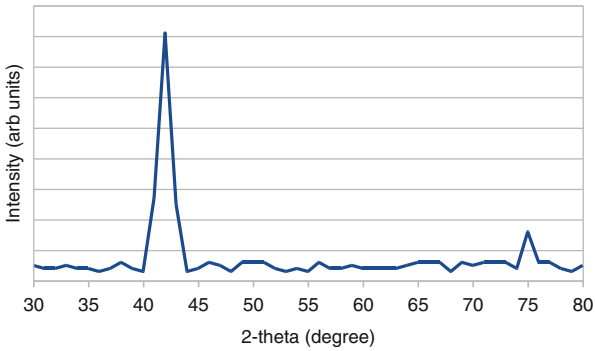

Fig. 17.4 Example of XRD spectra showing cubic diamond planes of (111) and (220)

Properties

Biological

The antibacterial properties of copper-doped DLC films have been evaluated against *Escherichia coli* (*E. coli*) [76]. *E. coli* were cultured on pure substrate, DLC film, and copper-doped DLC films, and then the antibacterial activity was calculated according to Eq. 17.1.

$$\text{antibacterial\_rate} = 100 * (\text{num\_bacteria}_{\text{control}} - \text{num\_bacteria}_{\text{tested}}) / \text{num\_bacteria}_{\text{control}} \tag{17.1}$$

The DLC film had an antibacterial rate of 40 %, and both of the copper-doped plates had an antibacterial rate of 100 % [76].

DLC films also have good biocompatibility; studies have shown these films do not invoke inflammation or cytotoxicity [88, 89]. Also, due to their tribological properties, they minimize thrombogenicity by minimizing platelet adhesion and activation [88]. By doping the films with nitrogen, their biocompatibility is improved due to the nitrogen supporting the attachment and proliferation of cells [89].

Electronic

There has been much interest in using DLC films as possible field electron emitters (FE). An FE is a device that emits electrons induced by an electrostatic field. These devices are used in electron guns for FE microscopy and in FE flat panel displays. It was initially thought that since DLC films have a negative electron affinity, they have the potential to serve as an FE without special preparation [90]. DLC films with a large (80 %) fraction of sp^3 bonds have the lowest threshold field for electron emission, of about 10 V μm^{-1} [90]. However, it was later discovered that surface roughness, not electron affinity, controls the field emission effects [90]. Due to quality control issues with developing DLC films and the superior properties of carbon nanotubes, DLC films are not currently being considered for use in industrial applications.

Mechanical

The internal stress in a DLC film is calculated by measuring the curvature of the substrate and film. The average internal stress in pure DLC films is 2.9 GPa [70, 71, 86]. When doped with Cu [86] or La_2O_3 [70] or ionized [71], the stress decreases. This is likely due to relaxing the bonds at the sp^3-sp^2 grain boundary. The internal stress is related to adhesion, and it should be noted that as the internal stress decreases, the adhesion of the DLC film to the substrate increases.

The strength of the adhesion (critical load) between the DLC film and the substrate is measured using a scratch tester. The critical load depends on the coating adhesive, the cohesive strength, and the frictional force between the diamond stylus and the coating. The median critical load of DLC films is 64 mN [70, 71, 74, 86]. The critical load is increased through doping or increasing the ion exposure of the DLC films. These methods decrease internal stress and cause the formation of a transition layer between the substrate and DLC film [70, 71, 86].

The hardness (toughness) of a DLC film is measured by indentation tests. These are usually conducted at enough of a load to significantly deform the film and the substrate. Pure DLC films had a hardness between 13 and 80 GPa, with an average hardness of 22 GPa [60, 67, 69, 70, 74, 77, 86]. When these films are doped with metals or annealed, the hardness decreases. DLC films doped with Cu had a hardness of 16 Gpa [86]. When DLC films were doped with tungsten, the hardness was reduced to 18 GPa [67]. After annealing to more than 1,000 K for 1 min, the hardness decreased to 14 GPa [60]. Much of the hardness depends on the ratio of sp^3 to sp^2 carbon within the DLC, so doped or annealed films should have a lower hardness as these types of films have an altered sp^3 to sp^2 ratio.

The elastic modulus measures the stiffness of the DLC films. For typical DLC films, the elastic modulus is approximately 180 GPa [67, 77]. When dopants are added to the DLC films, the elastic modulus changes depending on how the dopants affect the matrix. In the case of tungsten, it decreases [67]; when titanium is added, the elastic modulus increases, and as more titanium is added, the elastic modulus begins to decrease [77]. For films that consist of large amounts of sp^3 carbon, the elastic modulus is approximately 265 GPa [74].

The friction coefficient can be calculated using several different methods. Using scratch tests, DLC films have a friction coefficient that ranges between 0.19 [67] and 0.095 [70]. A copper-doped DLC film against a stainless steel ball has a friction coefficient of 0.15 [83]. As the amount of doped metal increases, the friction coefficient decreases [67, 70, 83].

Optical Properties

DLC films have good transmittance in the visible and IR range of the spectrum; however, in the UV portion of the spectrum, the transmittance drops off sharply due to the onset of fundamental absorption at the band gap of crystalline diamond (220 nm); see Fig. 17.5 [65, 68, 85]. This high transmittance indicates the suitability of DLC films for use in optical windows. Doping the DLC films with Ni or Cu ions causes the transmittance to decrease by half [65, 85]; a similar drop is seen when the films are annealed [68].

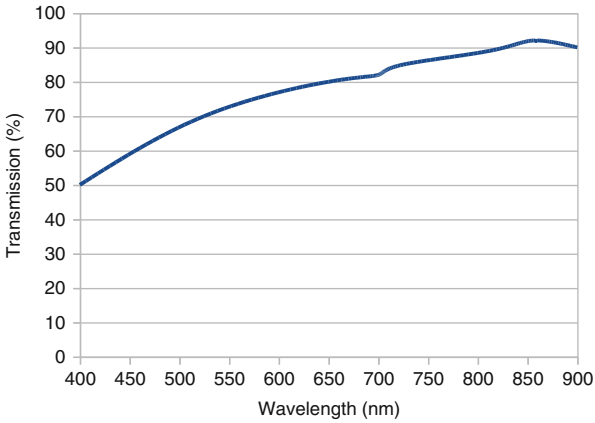

Fig. 17.5 Transmittance spectrum of representative DLC film

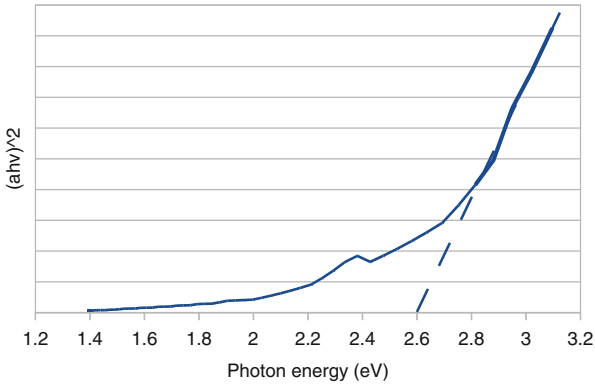

Fig. 17.6 Tauc plot showing extrapolated band gap

The optical band gap of DLC films can be calculated from the transmittance data, the Beer-Lambert law, and the Tauc relation [85]. The absorption coefficient, from the Beer-Lambert law, is given as Eq. 17.2:

$$a = \ln(1/\text{transmittance}) * (1/\text{path\_length}) \tag{17.2}$$

The optical band gap, E_g, is related to the absorption coefficient, a, by the Tauc relation, Eq. 17.3 [85]:

$$a = (A/h\nu)(h\nu - E_g) \tag{17.3}$$

In this equation, hν is the incident photon energy and A is the constant of proportionality. The constant of proportionality differs for different transitions. To determine the band gap, a plot of $(ah\nu)^2$ versus hν is created and the linear portion (near the transition energy) is extrapolated back to the x-intercept (a = 0);

see Fig. 17.6. This energy (hν) is the band gap. Since this technique depends on extrapolation, the estimated band gap can vary. For DLC films, the reported band gap is between 1.25 and 2.60 eV [65, 68, 85]. It is noted that the band gap decreases as the sp^3/sp^2 ratio decreases. The increase in sp^2 sites is indicative of graphitization within the films, which increases conductivity and hence reduces the band gap [68, 85].

References

1. Dolmatov VY (2001) Detonation synthesis ultradispersed diamonds: properties and applications. Russ Chem Rev 17:687–708
2. Gruen D, Shenderova O et al (2005) Synthesis, properties and applications of ultrananocrystalline diamond. Springer, Amsterdam
3. Shenderova O, Gruen D (2006) Ultrananocrystalline diamond: synthesis properties and applications. William-Andrew Publishing, Norwich
4. Shenderova OA, Zhirnov VV et al (2002) Carbon nanostructures. Crit Rev Solid State 27:227–356
5. Novikov NV (1999) New trends in high-pressure synthesis of diamond. Diamond Relat Mater 8:1427–1432
6. Lejosne J, Mercier G et al (2011) Low degree of functionalization of single-walled carbon nanotubes probed by highly sensitive characterization techniques. Carbon 49:3010–3018
7. Que R, Shao M, Chen T et al (2011) Diamond nanoparticles with more surface functional groups obtained using carbon nanotubes as sources. J Appl Phys 110:054321/1–054321/4
8. Voropaev S (2011) Cavitations synthesis of carbon nanostructures. J Phys Conf Ser 291:012028
9. Yang GW, Wang JB, Liu QX (1998) Preparation of nano-crystalline diamonds using pulsed laser induced reactive quenching. J Phys Condens Matter 10:7923
10. Wang JB, Zhang CY, Zhong XL, Yang GW (2002) Cubic and hexagonal structures of diamond nanocrystals formed upon pulsed laser induced liquid–solid interfacial reaction. Chem Phys Lett 361:86
11. Liang CH, Shimizu Y, Sasaki T, Koshizaki N (2003) Synthesis of ultrafine $SnO_{2a\text{-}x}$ nanocrystals by pulsed laser-induced reactive quenching in liquid medium. J Phys Chem B 107:9220
12. Liu QX, Wang CX, Zhang W, Yang GW (2003) Immiscible silver–nickel alloying nanorods growth upon pulsed-laser induced liquid/solid interfacial reaction. Chem Phys Lett 382:1
13. Yang GW, Wang JB (2000) Carbon nitride nanocrystals having cubic structure using pulsed laser induced liquid–solid interfacial reaction. Appl Phys A Mater Sci Process 71:343
14. Wang JB, Yang GW, Zhang CY, Zhong XL, Ren ZA (2003) Cubic-BN nanocrystals synthesis by pulsed laser induced liquid–solid interfacial reaction. Chem Phys Lett 367:10
15. Hanada K, Shoji T, Mayuzumi M et al (2004) Development of self-lubricating titania/diamond nanoparticle composite. Mater Sci Technol 20:1103–1108
16. Xu H, Yang Z, Li M-K et al (2005) Synthesis and properties of electroless Ni-P-nanometer diamond composite coatings. Surf Coat Technol 191:161–165
17. Koudoumas E, Kokkinaki O, Konstantaki M et al (2002) Onion-like carbon and diamond nanoparticles for optical limiting. Chem Phys Lett 357:336–340
18. Bilogurova L, Shevtsova M (2009) Investigation of the improvement of the physical and mechanical properties of polymer composite materials with nano-sized powders. Materialwiss Werkstofftech 40:331–333
19. Peng DX, Kang Y, Hwang RM et al (2009) Tribological properties of diamond and SiO_2 nanoparticles added in paraffin. Tribol Int 42:911–917
20. Gracias A, Tokranova N, Thelen BCM et al (2011) Influence of diamond nanoparticles on the thermal properties of benzocyclobutene (BCB). Phys Status Solidi A 208:684–690

21. Zhang Q, Mochalin VN, Neitzel I et al (2011) Fluorescent PLLA-nanodiamond composites for bone tissue engineering. Biomaterials 32:87–94
22. Tomita S, Fujii M, Hayashi S (2002) Optical extinction properties of carbon onions prepared from diamond nanoparticles. Phys Rev B Condens Matter 66:245424/1–245424/7
23. Ogata T, Yagi R, Nakamura N et al (2012) Modulation of polymer refractive indices with diamond nanoparticles for metal-free multilayer film mirrors. ACS Appl Mater Interfaces 4:3769–3772
24. Rozhkova NN, Gorlenko LE, Emel'yanova GI et al (2009) Effect of ozone on the structure and physicochemical properties of ultradisperse diamond and shungite nanocarbon elements. Pure Appl Chem 81:2093–2105
25. Mochalin VN, Neitzel I, Etzold BJM et al (2011) Covalent incorporation of aminated nanodiamond into an epoxy polymer network. ACS Nano 5:7494–7502
26. Fan J, Chu PK (2010) Group IV nanoparticles: synthesis, properties, and biological applications. Small 6:2080–2098
27. Perevedentseva EV, Su FY, Su TH et al (2010) Laser-optical investigation of the effect of diamond nanoparticles on the structure and functional properties of proteins. Quantum Electron 40:1089–1093
28. Cuche A, Sonnefraud Y, Faklaris O et al (2009) Diamond nanoparticles as photoluminescent nanoprobes for biology and near-field optics. J Lumin 129:1475–1477
29. Tizei LHG, Kociak M (2012) Spectrally and spatially resolved cathodoluminescence of nanodiamonds: local variations of the NV0 emission properties. Nanotechnology 23:175702/1–175702/8
30. Elouali M, Elouali FZ, Beyens C et al (2012) The effect of diamond nanoparticles on electro-optical properties of polymer dispersed liquid crystals. Mol Cryst Liq Cryst 561:136–144
31. Vlaeva I, Yovcheva T, Sainov S et al (2010) Optical properties of PVA films with diamond and titania nanoparticles. J Phys Conf Ser 253:012027/1–012027/6
32. Prosviryakov AS, Samoshina ME, Popov VA (2012) Structure and properties of composite materials based on copper strengthened with diamond nanoparticles by mechanical alloying. Met Sci Heat Treat 54:298–302
33. Baik E-S, Baik Y-J, Jeon D (2000) Aligned diamond nanowhiskers. J Mater Res 15:923–926
34. Ando Y, Nishibayashi Y, Sawabe A (2004) Nano-rods of single crystalline diamond. Diamond Relat Mater 13:633–637
35. Zou YS, Yang Y, Zhang WJ et al (2008) Fabrication of diamond nanopillars and their arrays. Appl Phys Lett 92:053105–053108
36. Wei M, Terashima C, Lv M et al (2009) Boron-doped diamond nanograss array for electrochemical sensors. Chem Commun 24:3624–3626
37. Szunerits S, Coffinier Y, Galopin E et al (2010) Preparation of boron-doped diamond nanowires and their application for sensitive electrochemical detection of tryptophan. Electrochem Commun 12:438–441
38. Coffinier Y, Galopin E, Szunerits S et al (2010) Preparation of superhydrophobic and oleophobic diamond nanograss array. J Mater Chem 20:10671–10675
39. Lin J-Y, Li Z-C, Chen C-Y et al (2011) Fabrication of submicron scale vertically aligned diamond rods by mask-free oxygen plasma etching. Diamond Relat Mater 20:922–926
40. Masuda H, Yanagishita T, Yasui K et al (2001) Synthesis of well-aligned diamond nanocylinders. Adv Mater 13:247–249
41. Sun L, Gong J, Zhu D et al (2004) Diamond nanowires from carbon nanotubes. Adv Mater 16:1849–1853
42. Gong JL, Sun LT, Zhu DZ et al (2006) Diamond nanowires from carbon nanotubes by hydrogen plasma treatment. Int J Nanosci 5:307–313
43. Dubrovinskaia N, Dubrovinsky L, Langenhorst F et al (2005) Nanocrystalline diamond synthesized from C60. Diamond Relat Mater 14:16–22
44. Rakha SA, Yu G, Zhou X et al (2009) Diamond nanowires from nanocrystalline diamond films. J Cryst Growth 311:3332–3336

45. Arenal R, Bruno P, Miller DJ et al (2007) Diamond nanowires and the insulator-metal transition in ultrananocrystalline diamond films. Phys Rev B 75:195431
46. Rakha SA, Yu G, Cao J et al (2010) Diamond-graphite nanowires produced by microwave plasma chemical vapor deposition. Diamond Relat Mater 19:284–287
47. Shenderova O, Brenner D, Ruoff RS (2003) Would diamond nanowires be stronger than fullerene nanotubes? Nano Lett 3:805–809
48. Ivanovskaya VV, Ivanovskii AL (2007) Atomic structure, electronic properties, and thermal stability of diamond-like nanowires and nanotubes. Inorg Mater 43:349–357
49. Barnard AS (2005) From nanodiamond to nanowires. In: Gruen DM, Shenderova O, Vul AY (eds) Synthesis, properties and applications of ultrananocrystalline diamond. Springer, Netherlands
50. Brenner DW, Shenderova OA, Harrison JA et al (2002) A second-generation reactive empirical bond order (REBO) potential energy expression for hydrocarbons. J Phys Condens Matter 14:783
51. Shenderova OA, Padgett CW, Hu Z et al (2005) Diamond nanowires. J Vac Sci Technol B Microelectron Nanometer Struct Process Meas Phenom 23:2457–2464
52. Barnard AS, Snook IK (2004) Phase stability of nanocarbon in one dimension: nanotubes versus diamond nanowires. J Chem Phys 120:3817–3821
53. Moreland JF, Freund JB, Chen G (2004) The disparate thermal conductivity of carbon nanotubes and diamond nanowires studied by atomistic simulation. Microscale Thermophys Eng 8:61–69
54. Padgett CW, Shenderova O, Brenner DW (2006) Thermal conductivity of diamond nanowires: molecular simulation and scaling relations. Nano Lett 6:1827–1831
55. Drory MD, Gardinier CF, Speck JS (1991) Fracture toughness of chemically vapor-deposited diamond. J Am Ceram Soc 74:3148–3150
56. Dubrovinskaia N, Dub S, Dubrovinsky L (2006) Superior wear resistance of aggregated diamond nanowires. Nano Lett 6:824–826
57. Richter A, Smith R, Dubrovinskaia N et al (2006) Mechanical properties of superhard materials synthesized at various pressure-temperature conditions investigated by nanoindentation. High Pressure Res 26:99–109
58. Zeng L, Peng H, Wang W et al (2008) Synthesis and characterization of diamond microcrystals and nanowires deposited by hot cathode direct current plasma chemical vapor deposition method. J Phys Chem C 112:6160–6164
59. Mousinho AP, Mansano RD, Salvadori MC (2010) Nanostructured diamond-like carbon films characterization. J Alloys Compd 495:620–624
60. Chung CK, Wu BH, Lai CW et al (2012) Nano silicon top-layer for composite-induced multiphasic enhancement of thermal stability of hardness of diamond-like carbon nanofilm at 900°C. Surf Coat Technol 206:4580–4584
61. Aisenberg S, Chabot R (1971) Ion-beam deposition of thin films of diamondlike carbon. J Appl Phys 42:2953–2958
62. Voevodin AA, Zabinski JS (1998) Superhard, functionally gradient, nanolayered and nanocomposite diamond-like carbon coatings for wear protection. Diamond Relat Mater 7:463–467
63. Hauert R, Patscheider J (2000) From alloying to nanocomposite - improved performance of hard coatings. Adv Eng Mater 2:247–259
64. Ma W, Liechtenstein VK, Szerypo J et al (2011) Preparation of self-supporting diamond-like carbon nanofoils with thickness less than 5 nm for laser-driven ion acceleration. Nucl Instrum Methods Phys Res A 655:53–56
65. Faizrakhmanov IA, Bazarov VV, Stepanov AL et al (2006) Effect of copper ion implantation on the optical properties and low-temperature conductivity of carbon films. Semiconductors 40:414–419
66. Wu W-Y, Ting J-M (2006) Growth and characteristics of metal-containing diamond-like carbon using a self-assembled process. Carbon 44:1210–1217

67. Bharathy PV, Yang Q, Kiran M et al (2012) Reactive bias target ion beam deposited W-DLC nanocomposite thin films – microstructure and its mechanical properties. Diamond Relat Mater 23:34–43
68. Sharda T, Rahaman MM, Nukaya Y et al (2001) Structural and optical properties of diamond and nano-diamond films grown by microwave plasma chemical vapor deposition. Diamond Relat Mater 10:561–567
69. Hayashi Y, Soga T (2004) Structural, optical and mechanical properties of nanostructure diamond synthesized by chemical vapor deposition. Tribol Int 37:965–974
70. Zhang Z, Lu X, Luo J et al (2007) Preparation and characterization of La_2O_3 doped diamond-like carbon nanofilms (I): structure analysis. Diamond Relat Mater 16:1905–1911
71. Palnitkar UA, Joseph PT, Niu H et al (2008) Adhesion properties of nitrogen ion implanted ultra-nanocrystalline diamond films on silicon substrate. Diamond Relat Mater 17:864–867
72. Wang C, Wang Q, Wang Z et al (2008) Nanocrystalline diamond embedded in hydrogenated fullerenelike carbon films. J Appl Phys 103:056110/1–056110/3
73. Luong JH, Male KB, Glennon JD (2009) Boron-doped diamond electrode: synthesis, characterization, functionalization and analytical applications. Analyst 134:1965–1979
74. Popov C, Favaro G, Kulisch W et al (2009) Influence of the nucleation density on the structure and mechanical properties of ultrananocrystalline diamond films. Diamond Relat Mater 18:151–154
75. Weng J, Xiong L, Wang J et al (2010) Effect of gas sources on the deposition of nanocrystalline diamond films prepared by microwave plasma enhanced chemical vapor deposition. Plasma Sci Technol 12:761–764
76. Chan Y-H, Huang C-F, Ou K-L et al (2011) Mechanical properties and antibacterial activity of copper doped diamond-like carbon films. Surf Coat Technol 206:1037–1040
77. Caschera D, Federici F, Pandolfi L et al (2011) Effect of composition on mechanical behaviour of diamond-like carbon coatings modified with titanium. Thin Solid Films 519:3061–3067
78. Brown IG (1998) Cathodic arc deposition of films. Annu Rev Mater Sci 28:243–269
79. Krishnaswamy J, Rengan A, Narayan J et al (1989) Thin-film deposition by a new laser ablation and plasma hybrid technique. Appl Phys Lett 54:2455–2457
80. Siegal MP, Barbour JC, Provencio PN et al (1998) Amorphous-tetrahedral diamondlike carbon layered structures resulting from film growth energetics. Appl Phys Lett 73:759–761
81. Foong YM, Hsieh J, Li X et al (2009) The study on the effect of erbium on diamond-like carbon deposited by pulsed laser deposition technique. J Appl Phys 106:064904/1–064904/8
82. Guo D, Cai K, Li L et al (2000) Preparation of hydrogenated diamond-like carbon films on conductive glass from an organic liquid using pulsed power. Chem Phys Lett 325:499–502
83. Huang L, Jiang H, Zhang J et al (2006) Synthesis of copper nanoparticles containing diamond-like carbon films by electrochemical method. Electrochem Commun 8:262–266
84. Wan S, Wang L, Xue Q (2010) Electrochemical deposition of sulfur doped DLC nanocomposite film at atmospheric pressure. Electrochem Commun 12:61–65
85. Pandey B, Hussain S (2011) Effect of nickel incorporation on the optical properties of diamond-like carbon (DLC) matrix. J Phys Chem Solids 72:1111–1116
86. Chen C-C, Hong FC-N (2005) Structure and properties of diamond-like carbon nanocomposite films containing copper nanoparticles. Appl Surf Sci 242:261–269
87. Hebert C, Ruffinatto S, Eon D et al (2013) A composite material made of carbon nanotubes partially embedded in a nanocrystalline diamond film. Carbon 52:408–417
88. Roy RK, Lee KR (2007) Biomedical applications of diamond-like carbon coatings: a review. J Biomed Mater Res B Appl Biomater 83:72–84
89. Liao WH, Lin CR, Wei DH et al (2012) Concurrent improvement in biocompatibility and bioinertness of diamond-like carbon films with nitrogen doping. J Biomed Mater Res A 100:3151–3156
90. Grill A (1998) Diamond-like carbon: state of the art. Diamond Relat Mater 8:428–434